THE ASTROPHYSICAL JOURNAL, 340:1049–1063, 1989 May 15

BOWEN FLUORESCENCE IN SCORPIUS X-1[1]

JONATHAN SCHACHTER,[2] ALEXEI V. FILIPPENKO,[3] AND STEVEN M. KAHN[2,4]
University of California, Berkeley
Received 1988 June 14; accepted 1988 October 25

ABSTRACT

We present the first measurements of O III Bowen fluorescence lines in near-ultraviolet spectra of the X-ray binary system Scorpius X-1. Our flux-calibrated spectra from the atmospheric limit ($\sim$3100 Å) to 1 μm also reveal the nitrogen Bowen lines near 4640 Å, the Balmer and Paschen series of hydrogen, the Paschen and Brackett series of He II, and numerous lines from Fe II and He I, among others. All of these lines probably arise in emission-line regions (ELRs) photoionized by X-rays produced near the neutron star surface. We use the observed line intensities to estimate explicitly the roles of the O1 and O3 channels of the Bowen cascades, as well as the possible importance of charge transfer between H I and O IV. Assuming the He II lines are produced by case B recombination, we derive a limit for the reddening toward Sco X-1 which agrees with previous determinations, although we show that the Brackett-Paschen line ratios for He II may not be consistent with case B production. We also use the Bowen line ratios (Bowen yields) to derive modest limits on the size (R_B) and density (n_e) of the Bowen ELR. We find $R_B \approx 10^{11}$–10^{12} cm, $n_e \approx 10^7$–10^{10} cm^{-3}. These results compare favorably with expectations, given the dimensions of the Sco X-1 binary system. We argue, however, that the accreting flow is much smaller than the He II Strömgren radius for the derived density, so that it is likely that the Bowen ELR is a low-density fringe of a much denser component of the system.

Subject headings: line formation — radiative transfer — stars: individual (Sco X-1) — ultraviolet: spectra — X-rays: binaries

I. INTRODUCTION

During the last 10–20 years, Bowen fluorescence (BF) has been studied in the Sun, planetary nebulae, X-ray bursters, X-ray binaries, and active galactic nuclei. BF is a line-transfer mechanism (Fig. 1) in which He II Lyα photons at 303.783 Å pump the nearly coincident O III $2p^2 \rightarrow 2p3d$ transitions at 303.799 and 303.693 Å (henceforth O1 and O3). The excited oxygen ion may decay through the $2p3p$ and $2p3s$ levels, in which case a number of near-ultraviolet Bowen lines (the strongest at 3133, 3429, and 3444 Å) are emitted, along with extreme ultraviolet (EUV) lines at shorter wavelengths. One of the subsequent EUV transitions (O III λ374.436, henceforth O4) is itself nearly coincident with the $2p \rightarrow 3d$ resonance doublet of N III. Hence, N III may also be excited and can decay via the $3p$ and $3s$ channels to yield optical Bowen lines ($\lambda\lambda$4097, 4103, 4634, 4641, 4642).

Although BF was first identified in the 1930s (Bowen 1934, 1935), it was not until accurate atomic physics data became available in the late 1960s that calculations of its efficiency and predicted spectrum were performed. Bowen first suggested BF to explain the appearance of anomalously strong O III and N III lines in the spectra of planetary nebulae. Indeed, subsequent detailed radiative transfer calculations by Weymann and Williams (1969) and Harrington (1972) have shown that BF is important for planetaries, owing to the large expected optical depths for the He II Lyα photons ($\tau_L \gg 10^5$) in the photoionized nebulae.

In more recent theoretical work, attention has focused on the relevance of BF to accretion-powered sources, specifically X-ray binaries (XRBs; McClintock, Canizares, and Tarter 1975; Kallman and McCray 1980; Deguchi 1985) and active galactic nuclei (AGNs; Eastman and MacAlpine 1985; Netzer, Elitzur, and Ferland 1985). For these cases, ambient gas surrounding the central compact object is photoionized by a hard, nonstellar continuum, as opposed to the softer stellar photospheric continuum expected from the central stars of planetary nebulae. The harder continuum has the effect of redistributing the ionization zones, so that several ionic species of each element can coexist in close proximity (Kallman and McCray 1982), possibly enhancing BF.

Optical and near-UV measurements of Bowen lines probe the transfer of the X-ray photoionizing continuum, so that an understanding of He II Lyα line transfer will complement the known X-ray properties of XRBs. For example, with a hard X-ray continuum, a K-shell (core) vacancy in a low-Z atom (e.g., O, N) may be followed by the radiationless emission of an L-shell (valence) electron. This process (the Auger effect) uses a single photon to convert a neutral species directly to the doubly ionized state; the resulting abundances of O III and N III influence BF.

The Bowen lines themselves are a sensitive and powerful diagnostic of physical conditions in accretion-powered sources, even without a detailed model. The Bowen yields, each defined as the intensity ratio of a line representing the cascade strength (e.g., λ3133) to one representing the pumping strength (e.g., λ4686), measure the efficiency of BF (see § V). For example, the He II–O III yield (y_{HeO}) reflects the probability that a He II Lyα photon will produce an O III Bowen line. As shown by Kallman and McCray (1980, hereafter KM80), y_{HeO} is only a function of the He II Lyα optical depth and the ratio of He II to O III abundances. With some simple and general assumptions about the ionization structure, one can derive constraints on the density, size, and location of the He II emitting region,

[1] Based on observations made at Lick Observatory, which is owned and operated by the University of California.
[2] Department of Physics and Space Sciences Laboratory.
[3] Department of Astronomy.
[4] Also affiliated with Laboratory for Experimental Astrophysics at Lawrence Livermore National Laboratory.

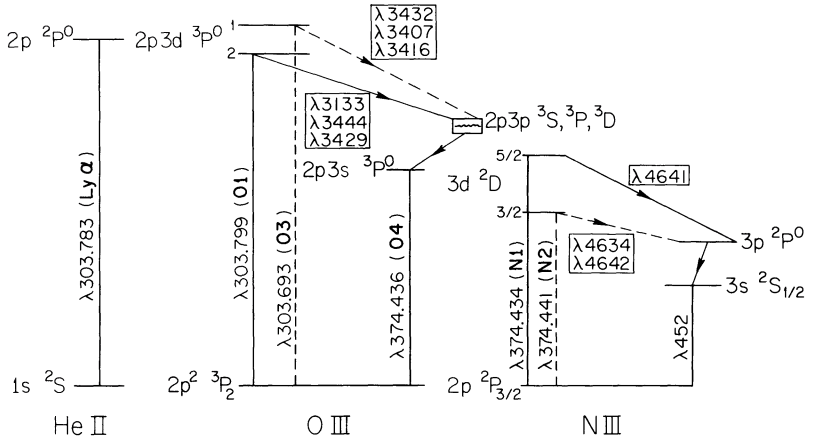

FIG. 1.—Grotrian diagram showing the principal pumping and cascade lines in Bowen fluorescence, with fine-structure energy-level separations exaggerated. The dashed lines are used to distinguish the O3 channel from the O1 channel and N2 from N1. Strong primary and secondary Bowen cascades are indicated with arrows, and wavelengths of predicted strong fluorescent lines are boxed.

relative to the central source. Both He II λ4686 and He II Lyα are presumably produced by recombination. Hence, an absolute measurement of λ4686 yields the Lyα luminosity, which provides additional constraints.

Despite growing recognition of the importance of BF in accretion-powered systems, the paucity of high signal-to-noise (S/N) ratio, flux-calibrated spectral observations of these sources down to the near-UV atmospheric limit at ~3100 Å has hindered further advances. Osterbrock (1981) and Shuder and Osterbrock (1981) detected O III Bowen lines in a few Seyfert nuclei, but only recently have absolute line fluxes become available (Malkan 1986). In near-UV spectra of compact Galactic X-ray sources, ozone absorption bands (3100–3400 Å) obscure the Bowen lines, severely compromising the accuracy of O III line fluxes. The lack of detectors sensitive down to the atmospheric limit has also hindered progress in the near-UV. However, two Galactic sources show clear evidence of O III lines: Margon and Cohen (1978) reported O III λ3444 in a photographic spectrum of Her X-1, while Oke and Greenstein (1971) detected λ3444 at low resolution in A0620−00 (= Nova Monocerotis 1975).

Fainter, southern sources may also possess Bowen emission, but these objects have rarely been observed below ~3500 Å. Canizares, McClintock, and Grindlay (1979, hereafter CMG) reported O III λλ3755, 3757, 3760, 3774, 3791 as part of a broad emission complex in the X-ray burster 4U 1735−44. The measured O III intensities relative to the N III Bowen lines are anomalously high, suggesting the presence of either the O3 process or charge transfer between H I and O IV (Sternberg and Dalgarno 1989; § V below). We discuss the CMG results further in § III. The broad complex may also be present in 4U 1636−53 and MXB 1659−29 (CMG), 2A 1822−371 (Charles, Thorstensen, and Barr 1980), and the transient burster Cen X-4 (Canizares, McClintock, and Grindlay 1980).

Emission at He II λ4686 together with a strong, broad blend near 4640 Å are detected in many Galactic X-ray sources, including Sco X-1 (Willis *et al.* 1980), Cyg X-2 (Bopp and Vanden Bout 1972), Her X-1 (Margon and Cohen 1978), A0620−00 (Whelan *et al.* 1977), and all the southern sources mentioned above. The 4640 Å blend may contain the Bowen lines of N III at 4634, 4641, and 4642 Å (produced by the O III–N III fluorescence), as well as lines from O II and C III (McClintock, Canizares, and Tarter 1975, hereafter MCT). Recently, Stripe, de Bruyn, and van Groningen (1988) have reported the detection of the 4640 Å blend in NGC 3783, which would make it the only known AGN with N III Bowen emission.

To explore the O III Bowen lines, we have undertaken a detailed study of BF in accretion-powered sources with the 3 m Shane reflector at Lick Observatory. Our sample includes narrow-line Seyfert 1 nuclei, Seyfert 2 nuclei, and low-mass Galactic XRBs. (In high-mass XRB systems, such as Cyg X-1, 4686 Å absorption in the early-type companion may contaminate the optical spectrum.) Here we present the first detection of O III Bowen lines in spectral observations of Sco X-1, the brightest XRB at X-ray wavelengths. We find that the strongest Bowen lines in Sco X-1 are O III λλ3133, 3444 and N III λλ4634, 4641, 4642. As this paper goes to press, we have just obtained another high-quality near-UV spectrum of Sco X-1. The results are generally consistent with those reported here; however, a detailed discussion of the more recent spectrum will be deferred to a subsequent paper.

We begin by discussing the instrumentation and our methods of data analysis (§ II). Detailed, flux-calibrated spectra of Sco X-1 are given in § III. An analysis of the reddening and distance to the source (§ IV) is followed by a consideration of the relevant atomic physics details, including the Bowen yields (§ V). In § VI we derive constraints on the size, density, and optical depth of the Bowen emission-line region (ELR). Our work is summarized in § VII.

II. OBSERVATIONS AND REDUCTIONS

Spectra were taken with the UV Schmidt system (Miller and Stone 1987), at the Cassegrain focus of the Lick 3 m Shane telescope, during three nights of reasonable seeing (1″.5–2″.5). Sco X-1, a southern object ($\delta_{1950} \approx -15^{\circ}.5$), was observed at air masses of 1.7–2.1. We obtained high-resolution, flux-calibrated spectra from the atmospheric limit at ~3100 Å to 1 μm, using three gratings. All objects were observed through a narrow (3″.2) slit at the six grating settings in Table 1. The 1200 groove mm^{-1} grating provides a dispersion of ~1 Å $pixel^{-1}$ in first order at the CCD detector (~4–5 pixel resolution); the

TABLE 1

GRATINGS, SETTINGS, AND FILTERS FOR BOWEN STUDY

Grating	Density (grooves mm^{-1})	λ_{blaze} (Å)	Setting	Range (Å)	Filter
1.....	1200	5000	UV	3100–3900	...
			Blue	3750–4550	...
			Green	4400–5200	...
2.....	600	5000	Orange	4700–6300	GG 385
			Red	5950–7550	GG 495
3.....	300	7500	IR	6600–9800	OG 570

dispersion of the others scales inversely with the groove density. A few spectra of flux standard stars were taken through larger apertures (10″) to check the absolute calibration. All six grating settings for Sco X-1 ($m_V = 12.4$) required a total of only 40 minutes of integration time, relatively short compared with the binary period (0.787 days; Gottlieb, Wright, and Liller 1975).

The high-resolution UV setting (Table 1) provides the O III Bowen lines as well as He II λ3204 (Paβ). The *green* setting, with even better resolution, gives the well-known (Sandage *et al.* 1966) broad 4640 Å feature, part of which is probably caused by the N III λλ4634, 4641, 4642 Bowen lines (MCT); it also includes Hβ and He II λ4686 (Paα). The *red* setting provides Hα for the Balmer decrement but avoids atmospheric A-band absorption (λ7600). To connect these three, we use the *blue* and *orange* settings. Finally, the *IR* setting probes the hitherto unexplored near-IR spectrum of Sco X-1. Because temporal variations were small in the intrinsic Sco X-1 spectrum during each 40 minute set of observations (see § V), the wavelength overlap from setting to setting (Table 1) provides a consistency check for our absolute fluxing. The filters used do not leak appreciably in second order.

Standard techniques (Filippenko and Sargent 1985) were used to extract one-dimensional spectra from the CCD data. These included subtraction of a bias level, division by a flat field, removal of cosmic rays, correction for geometric distortions and misalignments, and subtraction of background sky.

Obtaining flux-calibrated spectra in the near-UV down to the atmospheric cutoff presents a number of technical challenges. First, the detector must have high ($\gtrsim$25%) quantum efficiency (Q.E.) below 4000 Å, difficult to achieve in most available spectrographs. Second, one must consider atmospheric dispersion effects, which can selectively remove much of the light from the slit at these short wavelengths (Filippenko 1982). Finally, the absorption bands of atmospheric ozone (Huggins 1890) produce substantial modulation of the spectrum in the range 3100–3400 Å (Fowler and Strutt 1917). Other atmospheric bands, primarily O_2 and H_2O, are prominent in the red and IR ranges.

We have taken a number of steps in our observing program to alleviate these problems:

1. *Use of the Cassegrain CCD/UV–Schmidt system at the Lick* 3 m *reflector.*—The TI 800 × 800 pixel^2 CCD detector has exceptionally high near-UV Q.E. Flooded with UV light at room temperature, the CCD builds up electric charge that enhances its blue sensitivity (Djorgovski 1984; Mackay 1986), and is then cryogenically cooled with liquid nitrogen. Kept cold, it retains its high Q.E.

2. *Alignment of the slit along the parallactic angle.*—Dispersive losses can be minimized by orienting the slit along the angle of atmospheric refraction (Filippenko 1982). Except near the zenith, this angle changes relatively slowly with time for a given source; hence, we use the parallactic angle corresponding to the midpoint of the exposure, rather than updating the angle during the exposure. For example, during a 10 minute exposure of Sco X-1 crossing the meridian at air mass 1.68, the error in λ3133 intensity caused by a changing parallactic angle is ~1%. This is smaller than our estimated uncertainty in the continuum level.

3. *Removal of atmospheric absorption bands by division of spectra.*—Spectra of both Sco X-1 and a star which is featureless over the range of atmospheric absorption are taken at the same grating setting and similar air mass (when possible). During data reduction, we approximate the featureless continuum with a cubic spline. The observed spectrum lying below the spline forms an atmospheric absorption template, which is then scaled appropriately to the air mass of the Sco X-1 spectrum. Finally, the Sco X-1 spectrum is divided by the absorption template spectrum, revealing the intrinsic Sco X-1 features. See Wade and Horne (1988) for details of this procedure.

To remove ozone absorption from the 1987 May and June data (Table 2), we obtained near-UV spectra of Sco X-1, an sdF standard, *and* an sdO standard.[5] The sdF stars have intrinsic features at wavelengths shorter than ~3432 Å (the reddest ozone band), probably absorption from Fe I and other high-Z elements. Except for He II λ3204, however, the sdO stars show little evidence of intrinsic absorption in the range 3100–3500 Å. We therefore replace the 3204 Å portion of the sdO spectrum with the corresponding region of the sdF star, scaled appropriately to air mass. The resulting synthetic sdO star spectrum is the absorption template.

Our technique successfully removes much of the ozone absorption from the 1987 May 22 data, as shown in Figures 2*a* and 2*b*. Division highlights the O III Bowen lines in Sco X-1. The high-frequency noise in the final spectrum results from division by a spectrum with pixel-to-pixel noise. We discuss the near-UV Sco X-1 spectrum fully in later sections.

When dividing one spectrum by another, we require accurate wavelength calibration; otherwise, the results can be very noisy. Calibration arc lines of Hg, He, Ne, Ar, and Cd were used to set the wavelength scale. A linear or quadratic fit suf-

[5] The flux standards used in this work are Oke and Gunn (1983) sdF stars, together with sdO stars of Stone (1977). The sdF stars are poor flux standards in the range 3600–4000 Å, where Balmer-line absorption severely contaminates the continuum (e.g., Fig. 1 of Oke and Gunn 1983). The near-UV sdO continua, on the other hand, are relatively uncontaminated by Balmer absorption, so they make reliable flux standards.

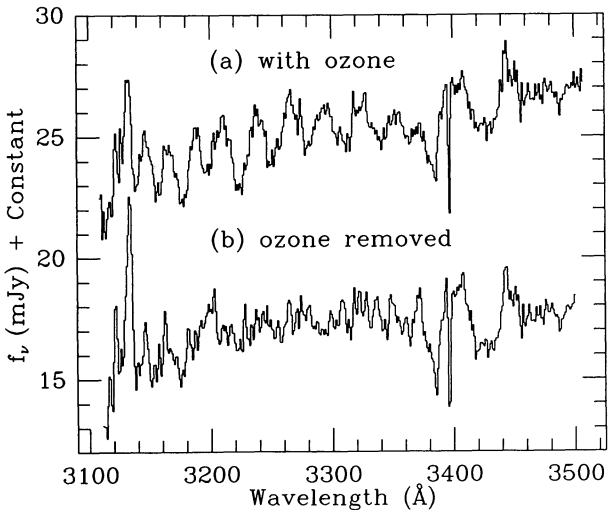

FIG. 2

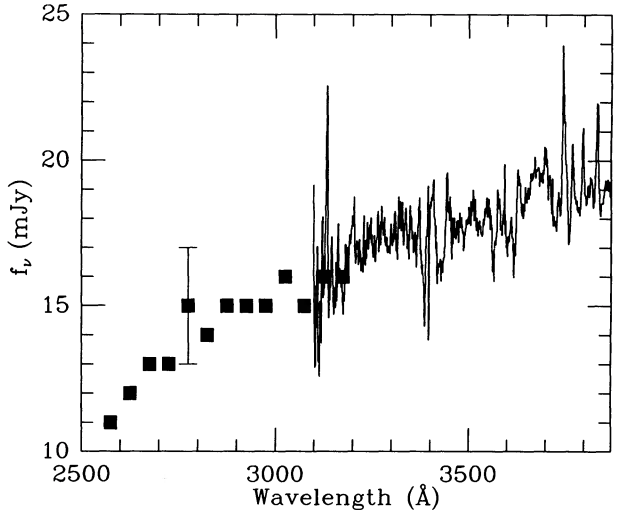

FIG. 3

FIG. 2.—UV spectra (1987 May 22) of Sco X-1 in the range 3100–3500 Å (*a*) before and (*b*) after removal of atmospheric absorption bands (§ II). In (*b*), O III λλ3133, 3444, the strong Bowen cascades, are evident. An offset of 10 mJy has been added to the spectrum in (*a*).

FIG. 3.—UV continuum of Sco X-1. The continuum in our 1987 May 22 Lick 3 m UV spectrum (*solid line*) is consistent with low-state, averaged broad-band (50 Å) UV fluxes derived from *IUE* data (*boxes*) of Sco X-1. An error bar represents typical statistical spread in individual *IUE* flux measurements.

ficed, with typical residuals ~0.1–0.2 of the pixel size. The UV Schmidt grating settings are, however, repeatable only to ~1 pixel (~1–4 Å). Occasionally, an encoder malfunction of which we initially were unaware produced significantly different (several to many Å) grating tilts for the same digital input. (This difficulty has now been remedied.) For this reason, we generally took an arc spectrum before or after each observation, especially when changing settings. When appropriate arc spectra were not available, we shifted the absorption bands of the template relative to Sco X-1 until a good division was obtained. Our method is essentially a cross-correlation by trial and error.

Despite the accurate calibration, observed wavelengths of strong lines in Sco X-1 differ from laboratory values by ~ 1–2 Å unless one takes into account the large (a few hundred km s^{-1}) velocities in the gas surrounding the accretion disk. In addition, the systemic velocity is large and negative (~ −140 km s^{-1} relative to the local standard of rest, according to Cowley and Crampton 1975), so that all the lines are expected to have an appreciable, uniform blueshift. Although the detailed velocity structure is unknown, our results appear to be consistent with previous observations (Crampton *et al.* 1976, hereafter CCHK).

III. NEW RESULTS

Flux-calibrated spectra of Sco X-1 were obtained on three nights (Table 2). In all cases, the spectral shape in regions of overlap (Table 1) was excellent, confirming that careful placement of the slit along the parallactic angle leads to minimal slit losses by atmospheric dispersion. Only small adjustments (a few %) in the *overall* continuum level had to be made in a few cases to ensure spectral continuity. Evidently, the atmospheric seeing and guiding changed very little while observations were being made. Our data from 1987 May 22 and low-state averaged *International Ultraviolet Explorer* (*IUE*) spectra (Willis *et al.* 1980) are combined in Figure 3. The agreement is good, indicating that our data give the correct flux down to the atmospheric limit. The *low* or *high* state of Sco X-1 (Table 2) refers to the measured *IUE* continuum level: the source can flare up to the higher state at any phase, and the typical high-state broad-band *IUE* flux is roughly twice that of the low state. (We assume for the moment that the intrinsic observable line and continuum spectrum in Sco X-1 remains constant from grating setting to setting; see § V for a discussion of the source variability.)

The complete 1987 May 22 Sco X-1 spectrum from the near-UV to near-IR is shown in Figure 4. Hα is by far the strongest emission line. Figure 5 illustrates the spectrum in more detail, using intervals of approximately 1000 Å. Note, in particular, the complexity of features blueward of the Balmer limit near 3650 Å (Fig. 5*a*). The spectra contain many emission lines, such as the Balmer and Paschen series of neutral H, He I λλ5876, 7065, He II λ4686, broad Fe II, and the O III and N III Bowen lines.

Line identification was performed with the aid of spectra of the Orion Nebula (Kaler, Aller, and Bowen 1965) and the planetary nebulae NGC 7027 (Aller, Bowen, and Minkowski 1955; Aller, Bowen, and Wilson 1963) and NGC 7009 (Kaler and Aller 1964), together with the comprehensive line list compiled by Kaler (1976). Energy levels are from Striganov and Sventit-

TABLE 2

LOG OF SCO X-1[a]

JD (−2,440,000)	Midpoint Time (UT)	Settings	Binary Phase	State
6937.88.....	1987 May 22 9:06	UV-IR	0.05	Low
6975.77.....	1987 Jun 29 6:27	UV-Green	0.18	Low
6976.83.....	1987 Jun 30 7:49	UV	0.52	High
6976.84.....	1987 Jun 30 8:13	UV	0.54	High

[a] Ephemeris from Gottlieb, Wright, and Liller 1975; *IUE* low or high state from Willis *et al.* 1980.

skii (1968), as are our quoted wavelengths for all but the Bowen cascades. Later authors occasionally differ from Striganov and Sventitskii by as much as 1 Å in the quoted wavelengths of the Bowen lines. The wavelengths we use for the O III O1 channel cascades are from Saraph and Seaton (1980, hereafter SS); those for the O3 cascades are from Deguchi (1985). A list of emission lines, primarily obtained from the 1987 May 22 data, is given in Table 3 together with absolute fluxes, uncorrected for reddening. The fluxes given are accurate to ~10%, except for $I(\lambda 3133)$ and $I(\lambda 3204)$ (~20%–30%). The distance and reddening of Sco X-1 are discussed in § IV. Subsections below examine the emission lines more fully.

a) Bowen Lines

Figure 5*a* indicates the presence of O III Bowen lines at 3133 and 3444 Å; atomic physics calculations predict these to be the strongest observable lines resulting from the decay of the excited O III ion (SS). Of additional interest is the emission blend peaking at ~3750 Å, far too strong to consist only of H12. A comparison with NGC 7027 suggests that N III $\lambda 3746$ is blended with H12. However, we would then predict N III $\lambda\lambda 3755$, 3771 to be present, since these two lines also result from the decay of the $3p\ ^4S_{3/2}$ level. N III $\lambda 3755$ is absent, although $\lambda 3771$ might conceivably be blended with H11.[6]

We used a Gaussian deblending program to separate the individual components of the H12 + N III $\lambda 3746$ blend. He II $\lambda 4686$ provides a template whose width is held fixed. Figure 6 shows a fit of two Gaussians, corresponding to N III and H12. The derived H12 intensity is consistent with the flat Balmer decrement (see below).

The possible presence of O III $\lambda 3407$ in the 1987 May 22 and 1987 June 30 data (Figs. 5*a*, 7*a*) suggests that the O III $2p3d\ ^3P^o$ state may be pumped by both O1 and O3 photons (Fig. 1). Of

[6] The southern source 4U 1735−44 is spectroscopically very similar to Sco X-1 in both the optical (McClintock, Canizares, and Backman 1978) and UV (Hammerschlag-Hensberge, McClintock, and van Paradijs 1982) spectral regions. We might, therefore, expect Sco X-1 to have the same O III Bowen lines in the range 3750–3780 Å reported in 4U 1735−44 (§ I; CMG). However, we would be unable to detect any of these lines in Sco X-1. In the absence of the O3 channel (see text below) or charge transfer (§ V), the strongest of these Bowen cascades (SS), $\lambda 3760$, is predicted to be only ~4% of $I(\lambda 3133)$. The predicted intensities of $\lambda\lambda 3774$, 3791 relative to O III $\lambda 3133$ (SS) are fantastically low, $\ll 1\%$, which completely eliminates the possibility of our detecting these lines in Sco X-1, assuming that the line widths are comparable to that of $\lambda 3133$. Further, the identification of the O III $\lambda\lambda 3774$, 3791 Bowen lines in 4U 1735−44 by CMG is probably wrong. From the CMG spectra, we have $I(\lambda 3791)/I(\lambda 4686) \approx 0.1$, which implies (SS) that $I(\lambda 3133)/I(\lambda 4686) \approx 100$, an unacceptably high Bowen yield (§ V).

TABLE 3

ABSOLUTE EMISSION-LINE INTENSITIES IN SCO X-1[a]

λ[b] (Å)	Identification	I_λ[c]	Notes	λ[b] (Å)	Identification	I_λ[c]	Notes
3133	O III	11.6		4641, 4642	N III	3.9	3
3204	He II	2.2		4647–52	C III	2.9	3
3407	O III	10.0		4686	He II	7.47	
3444	O III	3.5		4861	Hβ	14.4	
3478	He I	5.4	1	4922	He I	0.993	
3704	H15 + H16	1.91	1	5016	He I	1.20	
3722	H14	0.415	2	5412	He II	1.29	
3734	H13	1.03	3	5592	O III	<0.024	
3746	N III	6.6	3	5812	C IV	1.34	
3750	H12	2.8	3	5876	He I	4.77	
3771	H11	2.48		6347	Si II	0.799	
3798	H10	3.13		6371	Si II	0.502	
3835	H9	4.73		6563	Hα	45.7	
3867	He I	2.48		6678	He I	2.93	
3889	H8	6.50	4	7065	He I	2.97	
3970	H7	5.62	5	8438	P17 + P18	2.57	
4026	He I	1.25		8502	P16	2.69	
4102	Hδ	7.88		8545	P15	2.54	
4121	He I	0.611		8598	P14	1.80	
4200	He II	1.23	6	8665	P13	4.49	
4341	Hγ	8.37		8750	P12	3.23	
4471	He I	1.40		8863	P11	4.70	
4516	C III	1.71		9015	P10	4.53	
4542	He II	2.83		9229	P9	9.13	
4634	N III	2.0	3	9546	P8	9.58	

NOTES.—(1) Intensities from 1987 June 30 (see Table 8). (2) Intensities from 1987 June 29 (see Table 8). (3) Intensities from deblending analysis (see § III). (4) He I $\lambda 3888$ indistinguishable, probably weak. (5) He I $\lambda 3968$ also present. (6) Also may contain N III $\lambda\lambda 4195, 4200, 4215$.

[a] Not dereddened. Values from 1987 May 22, except as noted.

[b] Wavelengths from Striganov and Sventitskii 1968, except O III $\lambda 3407$ from Deguchi 1985; see § III.

[c] In units of 10^{-14} ergs cm^{-2} s^{-1}.

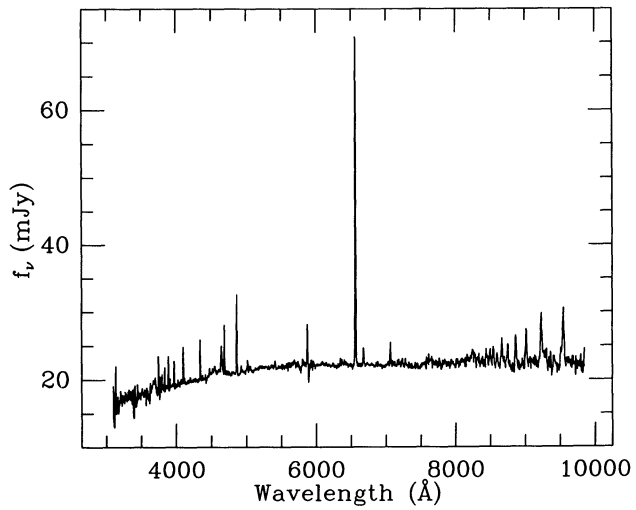

FIG. 4.—Complete spectrum of Sco X-1 from the near-UV to the near-IR, from 1987 May 22 data. Small differences in the overall flux level among different spectra have been adjusted, producing an overall smooth continuum.

the observable O3 cascades, λ3407 is predicted to be the second strongest; the strongest, λ3432, is not apparent in our spectra. For appreciable overlap between the He II Lyα and O3 profiles, we require a velocity width ~ 70 km s^{-1} (Deguchi 1985) within the scattering zone of each λ304 photon. (See further discussion in §§ V, VI.)

In Figure 7, spectra for the UV grating setting are presented at three different phases. While O III λλ3133, 3444 are present at all times, N III λ3746 (blended with H12) is detected only in the 1987 May 22 data—near zero phase—and O III λ3407 is detected in both the 1987 May 22 and June 30 data. Zero phase is defined as minimum light, presumably when the companion is in the line of sight to the compact primary.

The λ4640 broad blend, which contains N III Bowen lines at 4634, 4641, and 4642 Å, is also detected. This well-known complex has been seen previously in Sco X-1 (Sandage *et al.* 1966). Interpretation is more difficult than for O III, since the N III lines arise from the second BF step and are unresolved.

A three-Gaussian deblending analysis shows that the constituents of the blend are N III λ4634, N III λλ4641, 4642, and the *non*-Bowen blend C III λλ4647, 4651, 4652 (Fig. 8). The N III lines, all produced by O III–N III fluorescence, account for about two-thirds of the total blend intensity for both sets of observations (1987 May 22 and June 29). In § V we discuss the Bowen yields derived from these observations.

The observed N III *ratio*, which we define as $I(\lambda 4634)/I(\lambda\lambda 4641, 4642)$, may be compared with theory. Nussbaumer (1971) computed Einstein A coefficients for the N III EUV and optical lines in BF. To calculate the cascade probabilities and intensities, we assume that the $^2D_{5/2}$ and $^2D_{3/2}$ states of N III (Fig. 1) are equally populated; our results are given in Table 4. The theoretical N III ratio is 0.71. From our data, the derived N III ratios are 0.53 (for 1987 May 22) and 0.62 (for 1987 June 29), so that the observations agree well within our stated uncertainties.

b) He II

The most obvious He II line is λ4686 (Fig. 5*b*), the $n = 4$ to $n = 3$ transition or Paα. The next member in the series (Paβ) is He II λ3204, which, unfortunately, falls in a noisy part of the divided near-UV spectrum (Fig. 5*a*). If case B recombination applies to He II, then at $T = 10^4$ K and $n_e = 10^9$ cm^{-3} (§ VI), $I(\text{Pa}\beta)/I(\text{Pa}\alpha) \approx 0.5$ (Seaton 1978, extrapolated). From our observed intensities, and for $E_{B-V} \approx 0.1$–0.2 (§ IV), $I(\text{Pa}\beta)/I(\text{Pa}\alpha) \approx 0.4$. This result is consistent, within our observational error, with case B.

However, other processes may enhance the λ4686 intensity, which therefore affects the derived values of y_{HeO} (§ V) and E_{B-V} (§ IV). In AGNs, absorption of H Lyα (λ1215.67), which is nearly resonant with He II Hβ (λ1215.172), may preferentially populate the $n = 4$ level of He II (MacAlpine 1981). The resulting He II line intensities relative to λ4686, e.g., $I(\lambda 3204)/I(\lambda 4686)$, may differ significantly from case B recombination, as shown in AGN photoionization models of Netzer, Elitzur, and Ferland (1985). In § V we show $y_{\text{HeO}} = 0.5$–0.6 (near the KM80 saturated value) with case B assumed. Since $y_{\text{HeO}} \leq 1$ by definition, H Lyα pumping could conceivably account for ~40%–50% of the total observed λ4686 intensity in Sco X-1.

Other He II lines in our spectra provide additional information. We observe the Brackett series members λ4200 (Br11), λ4542 (Br9), and λ5412 (Brγ), with the last two contaminated by Fe II. The intensities of these lines relative to He II λ4686 are significantly higher than the case B values (Pengelly 1964 and Brocklehurst 1971, as cited in Osterbrock 1974). We find $I(\text{Br}\gamma)/I(\text{Pa}\alpha) = 0.14$ for $E_{B-V} = 0.2$ (§ IV), compared with 0.075 for case B. (The confusion with Fe II in the blue wing of Brγ may be partly responsible for the discrepancy.) With this assumed value for the reddening, our observed value of $I(\text{Br}11)/I(\text{Pa}\alpha)$ is higher than the case B result by a factor of ~11. These results suggest the possibility of considerable He II opacity in the Bowen ELR. Therefore, $I(\text{Pa}\alpha)/I(\text{Ly}\alpha)$ may exceed the case B ratio, and our derived value of y_{HeO} should be used as a lower limit. However, since y_{HeO} appears to be saturated in our measurements of Sco X-1, the derived size and density constraints are independent of the exact value of y_{HeO}.

We have clearly raised more questions about the He II line spectrum in Sco X-1 than we have answered. The effect of H Lyα pumping on $I(\lambda 4686)$ can be probed in future XRB models. Since the shape of the optical-IR extinction curve is well known, CCDs with high IR Q.E. should allow observations of He II Brα, so that $I(\text{Br}\alpha)/I(\text{Pa}\alpha)$ could be used as a reddening indicator. Eventually we will have good predictions of the He II line ratios. Since we currently lack this additional information, we will assume case B for the remainder of the paper, specifically pointing out the limitations imposed by this assumption in each instance.

TABLE 4

N III THEORETICAL LINE INTENSITIES[a]

λ (Å)	P_λ[b]	I_λ/I_{4641}
4634.....	5.4×10^{-3}	0.83
4641.....	6.5×10^{-3}	1.00
4642.....	1.1×10^{-3}	0.17

[a] Einstein A coefficients from Nussbaumer 1971.

[b] P_λ (cascade probability) normalized to unity for λ374 excitation.

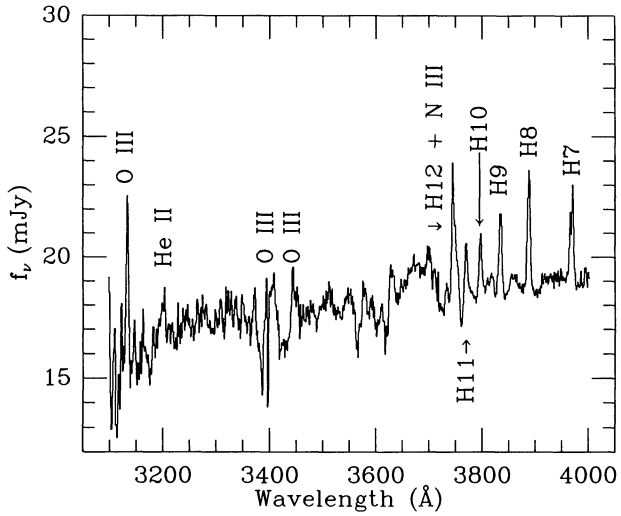

FIG. 5a

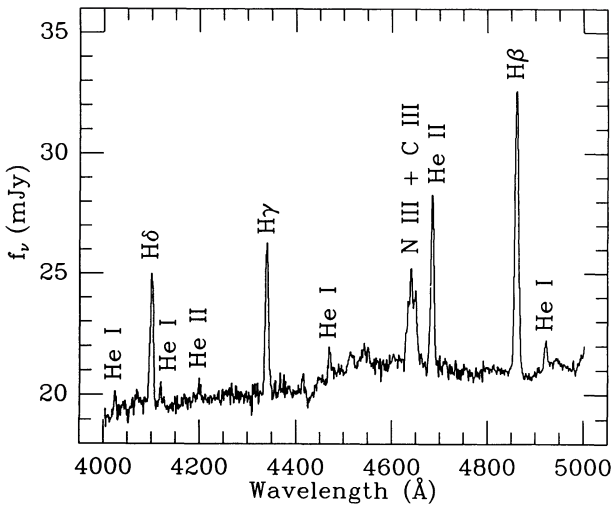

FIG. 5b

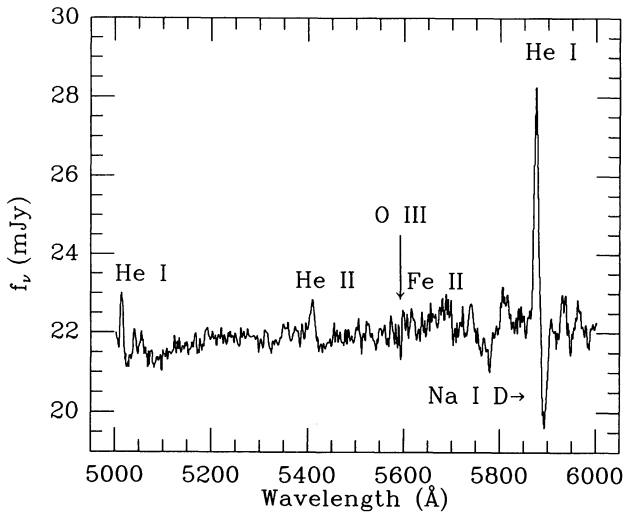

FIG. 5c

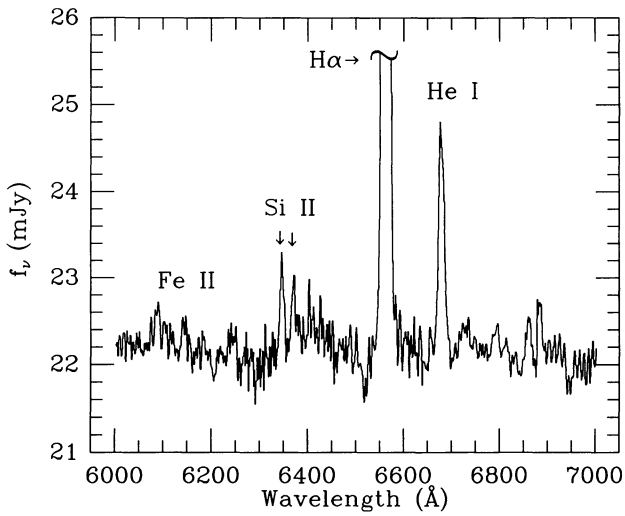

FIG. 5d

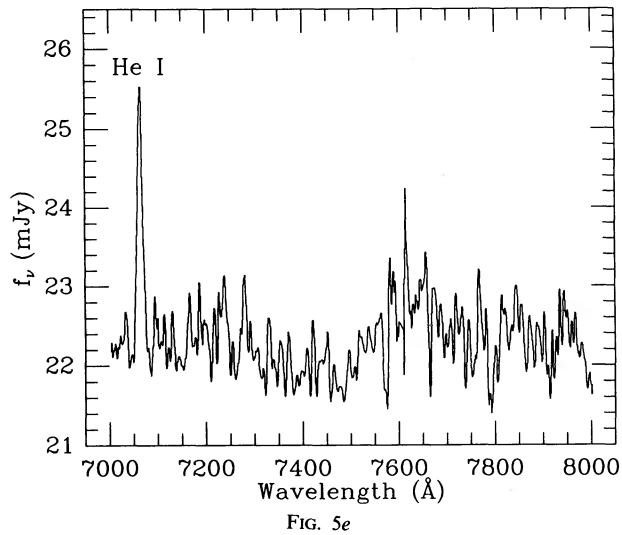

FIG. 5e

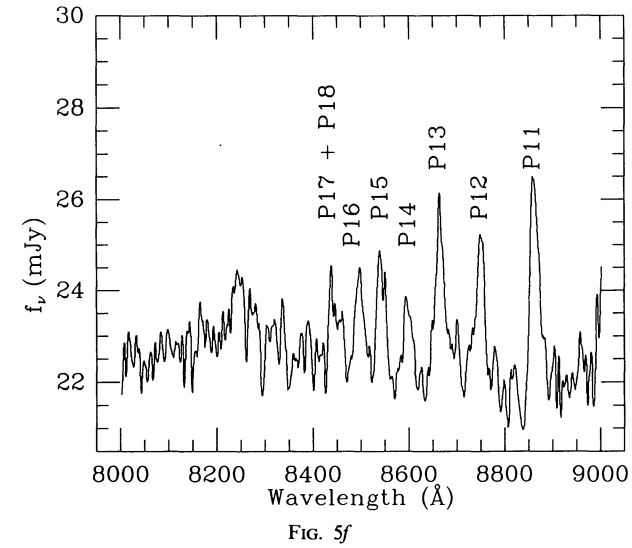

FIG. 5f

FIG. 5.—Complete spectra of Sco X-1 from near-UV to near-IR for 1987 May 22, in ~1000 Å sections. (*a*) 3100–4000 Å region. Contains Bowen lines at 3133 and 3444 Å. The Balmer series through H12 is evident; high-order lines are blended. (*b*) 4000–5000 Å region. Contains Bowen blend near 4640 Å (see § III), strong He II λ4686. Fe II present in this range. (*c*) 5000–6000 Å region. Fe II is visible. Expected location of O III λ5592 (produced by charge transfer, as described in § V) is indicated. (*d*) 6000–7000 Å region. Dominated by Hα, although Si II doublet and He I are present. Some Fe II is probably present. (*e*) 7000–8000 Å region. The only strong line is He I λ7065. (*f*) 8000–9000 Å region. Contains high-order Paschen lines.

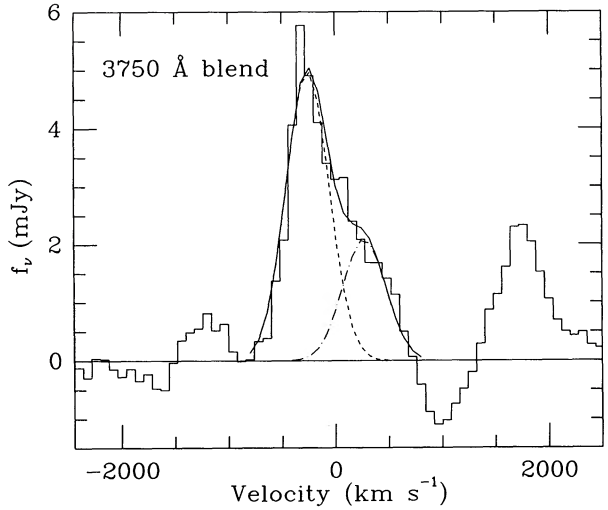

FIG. 6.—Fit to the 3750 Å blend using two Gaussians, with He II λ4686 as template having FWHM = 470 km s^{-1} (see § III). The deblended lines are N III λ3746 (*dashed line*) and H12 (*dot-dash line*), and the sum of the Gaussians (*solid line*) is also shown. The derived shape of H12 compares favorably with unblended H11, which is centered on ~ +1700 km s^{-1}. Derived heights of the Gaussians are (1) 4.9 mJy for N III (centered at −220 km s^{-1}) and (2) 2.0 mJy for H12 (centered at 310 km s^{-1}).

c) Fe II

Faint, unresolved multiplets of Fe II are present in Figures 5*b*, 5*c*, and 5*d*. The broad bump from 4400 to 4800 Å is probably caused by an Fe II λ4570 blend, containing multiplet numbers 37, 38, and 43. The similarity of this bump to that in Seyfert 1 nuclei (Phillips 1978) is encouraging. Nevertheless, Fe II λ5169 is absent, as are other members of multiplet 42 (λλ4924, 5018). However, these last two features may be blended with He I λλ4921, 5015. Weak lines of Fe II are probably present between He II λ5412 and He I λ5876, and between λ5876 and Si II λλ6347, 6371.

d) *Neutral Hydrogen*

The Balmer series is detected to high order (H14). Even higher members may be present in the broad feature between approximately 3720 Å and the Balmer limit (Fig. 5*a*). Some of the Balmer lines may be blended with other lines (see Table 3). The Balmer decrement is relatively flat, especially at the higher order members of the series. With $E_{B-V} = 0.2$ (§ IV), we have $I(\mathrm{H}\alpha)/I(\mathrm{H}\beta) = 2.5$, compared with 2.8 for case B. By contrast, $I(\mathrm{H}\gamma)/I(\mathrm{H}\beta) = 0.64$, for which case B gives 0.47. We therefore suggest that the H I ELR is optically thick in all Balmer lines, so the assumption of case B recombination is inappropriate for hydrogen.

Our near-IR data are the first to show lines of the H Paschen series (transitions to the $n = 3$ level) in Sco X-1 (Fig. 5*f*). The Paschen decrement is very flat; for example, the dereddened value of $I(\mathrm{Pa10})/I(\mathrm{H10})$ is ~2.2 times the case B value. Thus, the H I ELR is expected to have high opacity in all the Paschen lines. We can clearly identify higher order members through Pa18. The velocity widths of the Paschen and Balmer lines are similar.

e) *Other Emission and Absorption Lines*

We defer further discussion of the complex structure over the range ~3200–3400 Å to a future paper, in which we will present recently obtained near-UV Sco X-1 spectra. The 1987 May 22 spectra may contain O II λλ4415–4417 emission, possibly blended with Fe II. C IV λ5812 is marginally detected, and Si II λλ6347, 6371 are detected. Both the 1987 June 29 and June 30 spectra show He I λ3478 emission. In addition, the 1987 May 22 near-UV spectrum appears to contain absorption lines in the range 3580–3770 Å. A comparison with strong absorption lines in the solar spectrum (Moore, Minnaert, and Houtgast 1966) suggests identification with Fe I λλ3581, 3619, 3631, 3758. (Ni I λ3619 merges with Fe I λ3619.) A blend of Fe I λλ3764, 3767 is probably responsible for the broad absorption near λ3765. These lines may come from the companion, which is probably of late type, and perhaps somewhat evolved from the main sequence (Cowley and Crampton 1975, hereafter CC). On the other hand, the persistence of these absorption lines over the orbit would indicate their origin in the accretion-disk photosphere.

IV. REDDENING AND DISTANCE ESTIMATES

The reddening (E_{B-V}) toward Sco X-1 affects the calculation of Bowen yields (§ V), while the distance (D) to the source affects calculation of the He II Lyα luminosity. Neither E_{B-V} nor D is known precisely, but one can set some limits. The interpretation of reddening constraints is complicated by possible variations in the shape of the UV extinction curve along different lines of sight in the Galaxy. We therefore first present a brief review of interstellar UV extinction; Fitzpatrick and Massa (1986) discuss more details.

A general optical-UV extinction curve, where one plots extinction in magnitudes (A_λ) against λ^{-1} (e.g., Knude 1987), can be divided into three main parts: (1) a monotonically increasing optical portion, (2) a strong, broad (FWHM ≈ 400–600 Å) absorption bump near 2200 Å, and (3) a far-ultraviolet (FUV) monotonically increasing portion, usually flatter than the optical (e.g., Savage and Mathis 1979). The 2200 Å bump is probably caused by graphite grain absorption, while FUV extinction results from silicates (Greenberg and Chlewicki 1983).

At one time, it was thought that most stars obey a Galactic-averaged UV extinction curve (e.g., Nandy *et al.* 1975). The extinction toward σ Sco was a notable exception (Bless and Savage 1972). Later work showed large deviations along different lines of sight in FUV extinction, perhaps less in the 2200 Å bump (Meyer and Savage 1981; Cardelli and Savage 1988), indicating the desirability of star-specific UV extinction curves. The optical portion is more uniform (Massa 1980).

To probe the different components of UV extinction, Massa (1980) undertook a detailed photometric analysis of stars observed with the *TD-1* satellite (Boksenberg *et al.* 1973). In so doing, he discovered two independent components of extinction, which may represent two physical constituents. A general optical-UV extinction curve (f) can be written as a linear combination of the two components (f_1 and f_2) as

$$f(\lambda) = f_1(\lambda) \cos\theta + f_2(\lambda) \sin\theta \,. \quad (1)$$

Here the functions of θ represent the relative proportion of each component. Some general observational constraints on extinction and reddening yield $135° \leq \theta \leq 220°$.

We now consider two observational limits on the reddening toward Sco X-1, both of which rely on knowledge of its UV-optical extinction curve: first, the 2200 Å bump; second (a new approach for Sco X-1), the observed $I(\lambda1640)/I(\lambda4686)$ ratio.

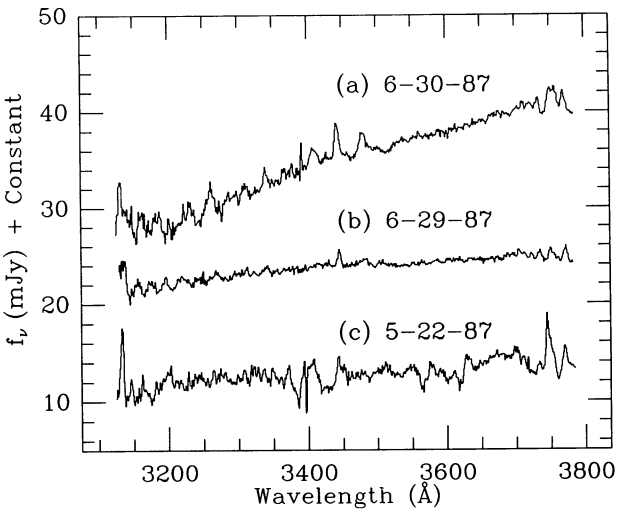

FIG. 7

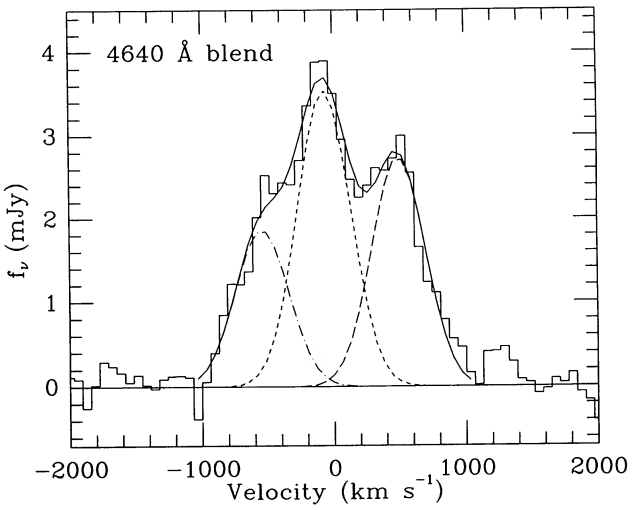

FIG. 8

FIG. 7.—UV spectra from three nights of observations of Sco X-1: (*a*) 1987 June 30, (*b*) 1987 June 29, and (*c*) 1987 May 22. Binary phase and other details are in Table 2. The high state near-UV continuum, shown in (*a*), is significantly redder than the low-state continuum, shown in (*b*) and (*c*). In the 1987 June 29 spectrum, part of the blue wing of O III λ3133 is lost because of a grating tilt controller problem (§ II). Additive offsets are +7 mJy for the 1987 June 29 spectrum, and −5 mJy for the 1987 May 22 spectrum.

FIG. 8.—Fit to the 4640 Å blend using three Gaussians, with He II λ4686 as template, as in Fig. 6. The deblended features are N III λ4634 (*dot-dashes*); N III λλ4641, 4642 (*short dashes*); and C III λλ4647, 4651, 4652 (*long dashes*). The sum of the fit Gaussians (*solid line*) is also shown. Derived heights of the Gaussians are (1) 1.9 mJy for N III λ4634 (centered at −620 km s^{-1}), (2) 3.6 mJy for N III λλ4641, 4642 (centered at −140 km s^{-1}), and (3) 2.7 mJy for C III (centered at 422 km s^{-1}).

a) 2200 Å *Interstellar Absorption Method*

Flux-calibrated optical spectra of Sco X-1 were unavailable before our study. The principal means of determining E_{B-V} has involved the strength of the 2200 Å feature in UV spectra of this source. The intrinsic UV continuum of Sco X-1, produced in the innermost regions of the accretion disk, is thought to be featureless throughout the spectral range ~1950–2450 Å. From spectra obtained with *IUE*, and the UV extinction curve of Nandy *et al.* (1975), Willis *et al.* (1980) derive $E_{B-V} = 0.35$ (Table 5). However, the dereddened spectrum is not an acceptably smooth UV continuum (Knude 1987).

This result may imply that the Nandy *et al.* curve poorly represents the UV extinction. As suggested above, many lines of sight deviate significantly from a Galactic-averaged UV extinction curve. More data on the extinction toward Sco X-1 are required to clarify this issue.

In this spirit, Knude (1987) constructed a reddening versus distance diagram for a field (Selected Area 132) centered near Sco X-1, based on *uvbyβ* photometry of approximately 200 stars. With these data and fluxes derived from 100 μm *Infrared Astronomical Satellite* (*IRAS*) measurements, Knude (1987) concluded that Sco X-1 may lie in an underreddened region. This is consistent with work of Meyer and Savage (1981), which shows that Sco X-1 lies in a region with lower than average 2200 Å absorption, and close to half the Galactic-averaged value for FUV extinction. In the FUV, the region has an extinction curve resembling that of σ Sco, an object ~10° away from Sco X-1. Using the σ Sco curve as a first approximation, the observed Sco X-1 2200 Å feature implies $E_{B-V} = 0.20$ (Knude 1987; Table 5).[7]

Based on the two-component UV extinction curves of Massa (1980) at $\theta = 200°$ and 220°, Knude (1987) derived even *smaller* values: $E_{B-V} \approx 0.11$ (Table 5). For $\theta = 200°$, the FUV extinction is similar to that of σ Sco, but the 2200 Å extinction is larger. The $\theta = 220°$ curve yields lower FUV extinction.

Thus, the depth of the 2200 Å bump indicates $0.11 \leq E_{B-V} \leq 0.20$ for three curves with low UV extinction. To determine the reddening more precisely, we now consider additional constraints imposed by our new optical data.

[7] We follow convention by quoting reddening in E_{B-V} magnitudes, although Knude actually calculated E_{b-y}. The two are related by $E_{B-V} = 1.35E_{b-y}$.

TABLE 5

SCO X-1 REDDENING FROM 2200 Å FEATURE[a]

Reference	Extinction Curve	E_{B-V}
Willis 1980	Nandy *et al.* 1975	0.35
Knude 1987	σ Sco	0.20
Knude 1987	Massa 1980, $\theta = 200°$	0.11
Knude 1987	Massa 1980, $\theta = 220°$	0.10

[a] Adapted from Knude 1987, Table 1. Units are magnitudes.

TABLE 6

SCO X-1 REDDENING FROM $I(\lambda1640)/I(\lambda4686)$[a]

Extinction Curve	$\Delta A/E_{B-V}$	E_{B-V} (May)	E_{B-V} (June)	Average E_{B-V}
Nandy *et al.* 1975	4.0	0.17	0.09	0.13
σ Sco	2.4	0.28	0.17	0.23
Massa 1980, $\theta = 200°$	2.6	0.26	0.15	0.21
Massa 1980, $\theta = 220°$	1.2	0.56	0.33	0.45

[a] References as in Table 5. $\Delta A = A_{1640} - A_{4686}$. "May" and "June" denote 1987 May 22 and June 29 (see Table 2). Units are magnitudes.

b) Method of He II $I(\lambda 1640)/I(\lambda 4686)$

A reddening indicator previously used only for AGNs (Netzer and Davidson 1979; Shuder and MacAlpine 1979; MacAlpine 1981) is the ratio of the intensity of He II $\lambda 1640$ (Balmer α) to that of He II $\lambda 4686$ (Paα). If $\lambda 1640$ and $\lambda 4686$ are both produced by case B recombination, then $I(\lambda 1640)/I(\lambda 4686) = 7.7$ at $T = 10^4$ K and $n_e = 10^9$ cm^{-3} (Seaton 1978, extrapolated). We now consider the relevant observations of He II $\lambda\lambda 1640$, 4686 in Sco X-1.

The $\lambda 1640$ intensity can be taken from *IUE* spectra of Sco X-1 in the low state (§ III), where we use the phase-averaged value because of the large observational scatter in individual measurements (Willis *et al.* 1980). The quoted uncertainty in the line intensity is 20%–30%. We combine this with our measurements of $\lambda 4686$ flux taken in the low state. With an assumed UV-optical extinction curve, we can use the intrinsic and observed $I(\lambda 1640)/I(\lambda 4686)$ ratios to constrain E_{B-V}. The constraints are really upper limits to E_{B-V} because of the possibility that the He II ELR is optically thick (see § III*b*).

The deduced reddening values are presented in Table 6 for our two different observations of $\lambda 4686$, with the extinction curves considered in the last section. While the Massa $\theta = 220°$ curve yields unacceptably *high* reddening, the rest imply $0.13 < E_{B-V} < 0.23$.

Note that the curves which give large values of E_{B-V} with the 2200 Å method in turn imply small E_{B-V} for the $I(\lambda 1640)/I(\lambda 4686)$ method. Only the σ Sco curve appears to give consistent results for both indicators. This strongly suggests that the correct reddening for Sco X-1 is $E_{B-V} \approx 0.2$.

c) Distance Estimates

The distance (D) to Sco X-1 is required to calculate the luminosity of $\lambda 4686$, which gives the unobservable He II $\lambda 304$ luminosity. A thorough summary of seven early distance determinations for Sco X-1 is given in Hiltner and Mook (1970). Some of these rely on data from other nearby stars. For example, Wallerstein (1967) showed that the Ca II K line equivalent width in Sco X-1 is larger than in five other stars near it in the sky, whence $D > 270$ pc.

The low $E_{B-V} = 0.11$ derived by Knude (1987) constrains the distance to $200 < D < 300$ pc. Every star in the Knude (1987) sample for which $D > 300$ pc has $E_{B-V} > 0.11$. Stars within 30′ of Sco X-1 have $E_{B-V} < 0.20$, which is closer to the above σ Sco result; they satisfy $D > 250$ pc.

An upper limit to D can be obtained independently from the measured maximum 2–12 keV flux (=20 mJy), as quoted in Giacconi *et al.* (1962). Assuming that the X-ray luminosity (L_x) must be less than the Eddington limit (L_E) for a 1.4 $M_\odot$ neutron star would require $D < 1.4$ kpc. We adopt $D = 700$ pc for the remainder of the paper, which corresponds to $L_x = L_E/4$ and is several times the lower limits above.

V. BOWEN YIELDS

The conversion efficiencies of He II and O III EUV photons into O III and N III fluorescent lines are measured by Bowen yields. In a model nebula photoionized by a central X-ray source, the assumed abundances lead to a relation between the Bowen yield and the pumping line opacity, e.g., τ_L for He II Lyα (Kallman and McCray 1980; Deguchi 1985). We will reverse the argument, and use existing models, together with our observed line strengths, to constrain τ_L (§ VI).

Here we define the Bowen yields in terms of strong observable lines which probe the corresponding EUV line intensities. They are (*a*) He II $\lambda 4686$, which measures He II Lyα; (*b*) O III $\lambda 3133$, which measures the O1 channel contribution to O III $\lambda\lambda 304$, 374; (*c*) O III $\lambda 3407$, which measures the O3 channel contribution to O III $\lambda\lambda 304$, 374; and (*d*) N III $\lambda\lambda 4634$, 4641, 4642, which measure the N III $\lambda 374$ doublet lines (N1, N2). As discussed earlier (§ I), the Bowen cascades are produced by the overlap of He II Lyα and O1. However, O3 can also be excited if sufficient (~ 70 km s^{-1}) velocity gradients are present (Deguchi 1985).

Since the Bowen yields are calculated from line intensities which are not obtained simultaneously, potential variability in the emission-line fluxes is an issue of genuine concern. Our observations at the various grating settings range from 5 to 20 minutes in duration, so that measurements of different lines used in yield calculations are separated by time scales of the order of $\frac{1}{2}$ hr. The underlying photoionizing spectrum in Sco X-1 is, in fact, known to be variable on time scales ranging from seconds (Petro *et al.* 1981) to hours (Kahn *et al.* 1981). However, several independent arguments suggest that the uncertainties introduced by source variability may not be severe: (1) The fractional variations are actually not very large on the relevant time scales. From the data presented by Holt *et al.* (1976), we estimate that the integrated X-ray flux for Sco X-1 typically varies by $\lesssim 30\%$, when binned on time scales comparable to our integration periods. (2) The emission-line fluxes cannot vary as fast or as dramatically as the X-ray flux in any case. Using the parameters derived below, we estimate the He II recombination time scale in the ELR to be $\sim 10^2$–10^4 s, significantly longer than the characteristic time scales for X-ray variability (Hudson, Peterson, and Schwartz 1970; Kestenbaum *et al.* 1971). (3) In addition, the consistency of our measurements for both lines and continuum in spectral regions where the settings overlap (§ III) is very good, $\lesssim$ a few percent. (4) Finally, the night-to-night variations in our deduced Bowen yields are again small, $\lesssim 10\%$–15%. Note that the 1987 June 29 value of $I(\lambda 3133)$, used in calculating the yields, is a (relatively firm) lower limit (Fig. 7*b*). Considering all these factors, we conclude that potential source variability probably cannot contribute more than a 20% error in our derived yields. This degree of uncertainty does not affect our conclusions, as shown below.

a) He II–O III Bowen Yield

The oxygen yield is defined as

$$y_{\mathrm{HeO1}} = k_{\mathrm{H}} \frac{I(\lambda 3133)}{I(\lambda 4686)}, \qquad (2)$$

where k_{H}, which depends on the (assumed case B) intensity ratio of $\lambda 4686$ to He II Lyα, decreases from 0.31 to 0.26 for

TABLE 7

BOWEN YIELDS IN SCO X-1 DERIVED FROM OPTICAL DATA[a]

Date (UT)	E_{B-V}	y_{HeO}	y_{ON}
1987 May 22	0.11	0.52	3.7
	0.20	0.59	3.2
1987 Jun 29	0.11	0.47	4.0
	0.20	0.54	3.5
1987 Jun 30	0.11	...	...
	0.20	...	...

[a] Bowen yields defined in § V.

TABLE 8

BOWEN AND RELATED LINE INTENSITIES IN SCO X-1[a]

Line	Date (UT)	I_λ(obs)	$I_\lambda(E_{B-V} = 0.11)$	$I_\lambda(E_{B-V} = 0.20)$
O III λ3133	1987 May 22	11.6	20.6	33.0
	1987 Jun 29	8.29	14.7	23.5
	1987 Jun 30	12.7	22.5	36.0
O III λ3407	1987 May 22	10.0	17.1	26.7
	1987 Jun 30	6.12	10.5	16.3
O III λ3444	1987 May 22	3.5	6.0	9.3
	1987 Jun 29	1.9	3.2	5.0
	1987 Jun 30	7.61	13.0	20.2
N III λ4634[b]	1987 May 22	2.0	3.0	4.2
	1987 Jun 29	1.7	2.6	3.6
N III λλ4641, 4642[b]	1987 May 22	3.9	5.9	8.2
	1987 Jun 29	2.8	4.2	5.9
He II λ4686	1987 May 22	7.47	11.2	15.6
	1987 Jun 29	5.80	8.70	12.1
Hβ λ4861[c]	1987 May 22	14.6	21.5	29.5
	1987 Jun 29	7.32	10.8	14.8

[a] In units of 10^{-14} ergs cm^{-2} s^{-1}.
[b] Intensities from deblending analysis (§ III).
[c] Given solely for comparison; intensity independent of Bowen process.

$T = (1–2) \times 10^4$ K (Harrington 1972). This yield is the probability that a He II Lyα photon is converted into an O1 channel Bowen cascade. If the O3 channel cascades were unambiguously detected (see § III), we would define $y_{\rm HeO3} = k_{\rm O3} I(\lambda3407)/I(\lambda4686)$, where $k_{\rm O3} = 0.33$ at $T = 10^4$ K, using the probability of producing λ3407 from Deguchi (1985). (See the discussion of the O3 contribution to N III cascades below.) We have used $I(\lambda3444)/I(\lambda3133) = 0.28$ from SS. For the rest of the discussion, we adopt $k_{\rm H} = 0.28$. The oxygen Bowen yields derived from our data are given in Table 7 and discussed in detail in § VI.

We present all our observed values of Bowen line intensities in Table 8, which also provides some information on the variability of the Bowen and related lines in Sco X-1 (see above). The quoted $I(\lambda3133)$ for 1987 June 29 is a relatively firm lower limit, since a grating tilt error (§ II) placed the blue wing of the line slightly off the edge of the detector (see Fig. 7*b*). Because of this, we find slightly lower values of $y_{\rm HeO}$ and larger values of $y_{\rm ON}$ (see below) compared with the data from 1987 May 22.

SS calculated intensities relative to λ3133 for the primary and secondary cascades of the O1 channel of the Bowen process (Fig. 1). The strongest observable *primary* cascades ($2p3d\ ^3P^o_2 \rightarrow 2p3p\ ^3S, ^3P, ^3D$) are at 3133, 3429, and 3444 Å, while the strong *secondary* cascades ($2p3p\ ^3S, ^3P, ^3D \rightarrow 2p3d\ ^3P^o$) are at 3341, 3312, and 3760 Å.

Of these, only λλ3133, 3444 are detected in our data. The observed value of $I(\lambda3444)/I(\lambda3133)$, which is relatively insensitive to the derived reddening (§ IV), is in reasonable agreement with the SS value of 0.28 for our 1987 May 22 and 1987 June 29 data (see Table 8). For 1987 June 30, where we measure $I(\lambda3444)/I(\lambda3133) \approx 0.56$, a slight red asymmetry in the profile of λ3444 suggests that it may be blended with He I λ3448. We have already reported a firm detection of He I λ3478, another singlet He I transition (§ III).

Deguchi (1985) determined the relative strengths of cascades produced by the O3 channel. The strongest observable primary lines ($2p3d\ ^3P^o_1 \rightarrow 2p3p\ ^3S, ^3P, ^3D$) are λλ3407, 3432, 3416, with secondary lines λλ3341, 3312, 3755. We find λ3407 in the 1987 May 22 and 1987 June 30 spectra.

Another process which can populate the excited O III levels is charge transfer (CT) between O IV and H I (Dalgarno and Sternberg 1982). By contrast with Bowen pumping of O III, CT populates only the $2p3p\ ^3S$ and ^3D states (Dalgarno, Heil, and Butler 1981). Thus, some secondary cascades have a contribution from both BF and CT. No secondary cascades are detected in our spectra, however.

We can quantify the importance of CT relative to BF by comparing the rates of population of the $2p3s\ ^3P^o_1$ level (Sternberg and Dalgarno 1989). In addition to the $2p3p\ ^3S$ and ^3D levels, CT would also populate the $2p3p\ ^1P$ level, resulting in λ5592 emission ($2p3p\ ^1P \rightarrow 2p3s\ ^1P^o$). This line has no Bowen contribution. Since (CT rate)/(BF rate) $\approx 40 I(\lambda5592)/I(\lambda3133)$, we find that CT has only a small effect (<4%) in Sco X-1.

b) O III–N III *Bowen Yield*

The nitrogen yield is given by

$$y_{\rm ON} = k_{\rm KM} \frac{I(\lambda\lambda4634, 4641, 4642)}{I(\lambda3133)}, \quad (3)$$

where $k_{\rm KM} = 8.6$, a constant that depends only on atomic physics parameters (KM80). This yield represents the fraction of O4 photons converted to an N III Bowen line. The derived N III yields (Table 7) are too large by a factor of ~3, since they measure probabilities ($y_{\rm ON} \leq 1$). However, based on § III, we have not included in equation (3) the O3 channel contribution to N III cascades. If both O1 and O3 channels contribute, we may write

$$y_{\rm ON} = \frac{I(\lambda\lambda4634, 4641, 4642)}{I(\lambda3133) f_{\rm O1}/k_{\rm KM} + I(\lambda3407)(1 - f_{\rm O1})/k_{\rm D}}, \quad (4)$$

where $k_{\rm D} = 0.75$ (Deguchi 1985), and $f_{\rm O1}$ measures the fraction of O4 photons produced by O1 excitation. To determine $k_{\rm D}$, we have used the calculated line-emission probabilities $P(\lambda3407) = 0.088$ and $P({\rm O4}) = 0.16$ from Deguchi (1985).

Given a model nebula, one can calculate the radiative transfer of O4 photons and derive $y_{\rm ON}$. The only such calculation we

know of which includes both O1 and O3 excitations is that of Deguchi (1985). He finds that $y_{ON} \approx 1$ at saturation (when y_{ON} is normalized to unity O4 production efficiency). Equation (4) and our measured line strengths then imply $f_{O1} = 0.6$–0.7 for $E_{B-V} = 0.1$–0.2. The Deguchi (1985) calculation contains a low abundance of continuum absorbers (e.g., $n_{N\,III}/n_{He\,I} \approx 5$), which may account for the large y_{ON} (cf. KM80, eq. [23]). It also assumes extreme velocity gradients (§ VI). However, since $y_{ON} \leq 1$ for any calculation, we may regard our value for f_{O1} as a (weak) upper limit. Future detection of O3 primary cascades in Sco X-1 would strengthen this argument.

In conclusion, $I(\lambda 3133)/I(\lambda 3444)$ in Sco X-1 agrees with SS over the range of our observations. Charge transfer is probably unimportant, whereas the O3 Bowen channel may contribute, particularly to the N III cascades.

VI. DISCUSSION

Our Bowen observations probe He II $\lambda 304$ in Sco X-1 in two ways. First, the absolute measured intensity of He II $\lambda 4686$ is related to the $\lambda 304$ flux, since both lines are believed to be produced by recombination. Second, the measured Bowen yields (y_{HeO} and y_{ON}) can be used to place lower limits on the corresponding pumping line optical depths (τ_L and τ_{O4}).

KM80 give the basic dependence of y_{HeO} on τ_L for a quasi-static nebula in which thermal Doppler broadening predominates. They estimate a critical value of $\tau_L (= \tau_{crit})$ for the Bowen process to work:

$$\tau_{crit} = 80 \frac{n_{He\,II}}{n_{O\,III}} . \tag{5}$$

For $\tau_L < \tau_{crit}$, escape of the Lyα photon from the nebula precludes Bowen cascade production. We find $\tau_{crit} \approx 10^4$ for a typical X-ray nebular model (see below). The value of y_{HeO} at τ_{crit} is ~ 0.45. Over the range $1 \leq \tau_L/\tau_{crit} \leq 10$, y_{HeO} is a steeply increasing function of τ_L. At higher values of τ_L (10–100), $y_{HeO}(\tau_L)$ flattens as photoelectric absorption starts to compete with Lyα escape. Since this continuum absorption (by H I, He I) is largely insensitive to τ_L, y_{HeO} saturates at

$$y_{HeO}^{sat} \approx \frac{1}{1 + 2 \times 10^{-3} n_A / n_{O\,III}} , \tag{6}$$

where n_A is the number density of absorbers, expressed as an equivalent H I density. The value of y_{HeO}^{sat} so derived assumes that continuum absorption becomes important at ~ 10 Doppler widths from Lyα line center. Assuming our observed $y_{HeO} = y_{HeO}^{sat}$, we find $n_A/n_{O\,III} \approx 10^2$, which agrees reasonably well with the X-ray nebular model. We will therefore assume that y_{HeO} is saturated.

For an XRB, Deguchi (1985) has suggested that bulk velocity gradients may affect the line overlap of He II and O III. However, a simple calculation shows that this is probably *not* a complication for the problem at hand. Velocity gradients can seriously influence the line transfer only if the mean diffusion distance (l_d) of a Lyα photon between creation and Bowen conversion (or escape) significantly exceeds the characteristic distance (l_V) over which the average velocity shift is comparable to the thermal velocity. As shown by KM80, most of the Bowen conversion occurs in the Doppler core of the Lyα line, where complete frequency redistribution applies. In this case, at low optical depths, the mean number of scatterings ($\bar{N}$) experienced by a given line photon is $\bar{N} \approx \tau_0 (\pi \ln \tau_0)^{1/2}$, where τ_0 is the optical depth at line center (see discussion by Adams 1972). When $\tau_0 \geq \tau_{crit}$, however, Bowen conversion dominates over escape, and $\bar{N}$ saturates at the value

$$\bar{N} \approx \tau_{crit} (\pi \ln \tau_{crit})^{1/2} . \tag{7}$$

The mean diffusion distance is then given by

$$l_d \approx \bar{N}^{1/2} \frac{R}{\tau_0} , \tag{8}$$

where R is the characteristic size of the region.

The typical distance associated with the velocity gradient (∇V) is given by

$$l_V \approx \frac{V_{th}}{|\nabla V|} , \tag{9}$$

where V_{th} is the thermal velocity of the helium ion. For accretion flows around a compact object of mass M,

$$|\nabla V| \approx \left(\frac{GM}{r^3} \right)^{1/2} , \tag{10}$$

where r is the distance from the central star to the center of the ionized region. We thus find

$$\frac{l_d}{l_V} \approx \frac{\tau_{crit}^{1/2} (\pi \ln \tau_{crit})^{1/4}}{\tau_0} \left(\frac{R}{r} \right) \left(\frac{GM}{rc^2} \right)^{1/2} \left(\frac{V_{th}}{c} \right)^{-1} . \tag{11}$$

Assuming $M = 1.4\,M_\odot$, $T \approx 10^4$ K, and $r \approx 10^{11}$ cm (see discussion below), we find

$$\frac{l_d}{l_V} \approx 280 \frac{\tau_{crit}^{1/2} (\pi \ln \tau_{crit})^{1/4}}{\tau_0} \left(\frac{R}{r} \right) . \tag{12}$$

Our derived Bowen yields in Sco X-1 are near the maximum estimated by KM80, so $\tau_0 \geq 100 \tau_{crit} = 10^6$. Also, $R \leq r$, hence

$$\frac{l_d}{l_V} \leq 6 \times 10^{-2} . \tag{13}$$

This implies that typical accretion velocity gradients have little influence on the line transfer. We therefore use the KM80 calculations and assume an optical depth defined in terms of the thermal velocity.

The Bowen ELR size (R_B) and number density of He II ($n_{He\,II}$) can be estimated from τ_L and $I(\lambda 4686)$ (Deguchi 1985). For case B recombination at $T = 10^4$ K, $I(\mathrm{Pa}\alpha)/I(\mathrm{Ly}\alpha) \approx 0.3$:

$$N_{\mathrm{Pa}\alpha} = 0.3 \alpha_B n_e n_{He\,III} \tfrac{4}{3} \pi R_B^3 \ \mathrm{s}^{-1} , \tag{14}$$

where $N_{\mathrm{Pa}\alpha}$ is the number of photons emitted per second in $\lambda 4686$, and α_B is the radiative recombination coefficient to levels $n \geq 1$.[8] From Gould and Thakur (1970), $\alpha_B = 2.3 \times 10^{-12}$ cm^3 s^{-1}, assuming case B recombination for the determination of the Gaunt factor. If $n_e/n_{He\,II}$ and $n_{He\,III}/n_{He\,II}$ are known, equation (14) provides the He II emission measure.

The opacity is given by

$$\tau_L \approx n_{He\,II} \sigma_L R_B , \tag{15}$$

where $\sigma_L = 2.94 \times 10^{-14}$ cm^2 for a Doppler profile at $T = 10^4$ K (e.g., Rybicki and Lightman 1979, eq. [10.71]).

[8] If the Bowen ELR is optically thick in the He II Balmer lines (§ III*b*), we may write $N_{\mathrm{Pa}\alpha} = 0.3 f_\tau \alpha_B n_e n_{He\,III} (4/3) \pi R_B^3$, where we expect $f_\tau \approx 1$–2 (Davidson and Netzer 1979, § IV*c*). The corresponding upper limit on the emission measure, when coupled with the lower limit on Lyα opacity, does not significantly alter the derived constraints on R_B, n_e, and $r_{He\,III}$.

Stimulated emission is neglected, and most of the He II is assumed to be in the ground state. Solving for R_B and $n_{He\,II}$, we find

$$R_B \approx 3.0 \times 10^{15} \frac{N_{44}}{\tau_6^2 x_{He\,III} x_{e10}} \text{ cm} \quad (16)$$

and

$$n_{He\,II} \approx 1.1 \times 10^4 \frac{\tau_6^3 x_{He\,III} x_{e10}}{N_{44}} \text{ cm}^{-3}, \quad (17)$$

where $10^{44} \times N_{44}$ is the number of photons per second in λ4686, τ_6 is the Lyα optical depth in units of 10^6, and $x_{He\,III} = n_{He\,III}/n_{He\,II}$, $x_{e10} = n_e/10n_{He\,II}$ are the abundances.[9] Based on the foregoing discussion, we have used the thermal velocity for He ($=6.4 \times 10^5$ cm s^{-1} at $T = 10^4$ K) to calculate the line width. As in KM80, τ_{crit} depends on the He II and O III abundances; the value 10^6 corresponds to the onset of y_{HeO} saturation.

The above relationships (eqs. [16] and [17]) can be scaled to our data. We state them as inequalities, based on the requirement that the y_{HeO} curve is flat to $\sim$1%, which implies $\tau_6 \geq 1$ (Kallman 1988). We have

$$R_B \leq 3.8 \times 10^{12} \frac{I_{12} D_{700}^2}{\tau_6^2 x_{He\,III} x_{e10}} \text{ cm} \quad (18)$$

and

$$n_{He\,II} \geq 8.7 \times 10^6 \frac{\tau_6^3 x_{He\,III} x_{e10}}{I_{12} D_{700}^2} \text{ cm}^{-3}, \quad (19)$$

so that

$$n_e \geq 8.7 \times 10^7 \frac{\tau_6^3 x_{He\,III} x_{e10}^2}{I_{12} D_{700}^2} \text{ cm}^{-3}, \quad (20)$$

where I_{12} is the λ4686 intensity in units of 12×10^{-14} ergs cm^{-2} s^{-1}, and D_{700} is the distance to the source in units of 700 pc.

We now derive complementary constraints from the requirement that the spontaneous radiative decay rate from the $n = 2$ level of He II exceed the collisional de-excitation rate. For a transition in a two-level atom (or ion) from level j to level i, one can define a critical electron density (n_c) such that the collisional de-excitation rate (C_{ji}) balances the radiative decay rate (A_{ji}); hence, $n_c = A_{ji}/C_{ji}$. If the transition is a resonance line such as He II Lyα, at large line-center optical depth τ_0, collisional de-excitation is enhanced by the number of scatterings, $\sim 6\tau_0$. One therefore finds for this case $n_c \approx A_{ji}/(6C_{ji}\tau_0)$ (see Davidson and Netzer 1979, § IV*a* and references therein). From the approximate formula of Mewe (1972), we obtain $C_{21} = 6.24 \times 10^{-9}$ cm^3 s^{-1} for He II at $T = 10^4$ K. Thus,

$$n_c \tau_0 = 2.7 \times 10^{17} \text{ cm}^{-3} > n_e \tau_L, \quad (21)$$

which is a strict upper limit. (Because $n_c \tau_0 \propto Z^6$ for hydrogenic species, the value for He II is considerably larger than for H Lyα.) From formula (20), we find

$$n_e \tau_L = 8.7 \times 10^{13} \frac{\tau_6^4 x_{He\,III} x_{e10}^2}{I_{12} D_{700}^2} < 2.7 \times 10^{17} \text{ cm}^{-3}, \quad (22)$$

so that

$$\tau_6 < 7.5 \frac{I_{12}^{1/4} D_{700}^{1/2}}{x_{He\,III}^{1/4} x_{e10}^{1/2}}. \quad (23)$$

Thus, the constraints are

$$R_B > 6.8 \times 10^{10} \frac{I_{12}^{1/2} D_{700}}{x_{He\,III}^{1/2}} \text{ cm} \quad (24)$$

and

$$n_e < 3.7 \times 10^{10} \frac{x_{He\,III}^{1/4} x_{e10}^{1/2}}{I_{12}^{1/4} D_{700}^{1/2}} \text{ cm}^{-3}. \quad (25)$$

The deduced values for the Bowen ELR size may be compared with known length scales in the Sco X-1 system. CC showed that the projected distance of the primary from the center of mass ($a_1 \sin i$, where i is the inclination) is of order 6×10^{10} cm. From the wings of He II λ4686 profiles, CCHK inferred a maximum radial velocity $\sim$1500 km s^{-1}. If its velocity profile is close to Keplerian, the ELR radius would then be $\sim 10^{10}$ cm. The size of the Roche lobe of the primary, with $i \approx 30°$ and representative masses, is $\sim 10^{11}$ cm (CC). If we demand $R_B < 10^{11}$ cm, then

$$\tau_6 > 6.2 \frac{I_{12}^{1/2} D_{700}}{x_{He\,III}^{1/2} x_{e10}^{1/2}}, \quad (26)$$

so that

$$n_e > 2.1 \times 10^{10} \frac{x_{e10}^{1/2} I_{12}^{1/2} D_{700}}{x_{He\,III}^{1/2}} \text{ cm}^{-3}. \quad (27)$$

Kallman and McCray (1982) constructed models for nebulae photoionized by central compact X-ray sources. Their model 6 is a spherically symmetric gas cloud, ionized by a 2 keV thermal bremsstrahlung spectrum with $L = 10^{37}$ ergs s^{-1} and $n_e = 10^{11}$ cm^{-3} (similar to Sco X-1). As in Kahn, Seward, and Chlebowski (1984), the Strömgren radius of the He III region is given by

$$r_{He\,III} = 2.2 \times 10^{12} \frac{L_{37}^{1/3}}{n_{e11}^{2/3}} \text{ cm}, \quad (28)$$

where L_{37} is the X-ray luminosity in units of 10^{37} ergs s^{-1} and n_{e11} is the electron density in units of 10^{11} cm^{-3}. Substituting the constraints on n_e from equations (20) and (25) yields

$$r_{He\,III} < 2.5 \times 10^{14} \frac{L_{37}^{1/3} D_{700}^{4/3} I_{12}^{2/3}}{x_{He\,III}^{2/3} x_{e10}^{4/3}} \text{ cm}, \quad (29a)$$

$$r_{He\,III} > 4.3 \times 10^{12} \frac{L_{37}^{1/3} D_{700}^{1/3} I_{12}^{1/6}}{x_{He\,III}^{1/6} x_{e10}^{1/3}} \text{ cm}. \quad (29b)$$

Note that the derived lower limit on the He III Strömgren radius is still significantly larger than the characteristic dimension of the binary system quoted above. Hence, it would not be possible to maintain the ELR as an isolated cloud within the region believed to contain the accreting flow. It seems more likely that the ELR is a low-density fringe of a denser structure located within the system at $r \approx 10^{11}$ cm.

[9] Note the correct dependences on τ_L: $R_B \propto \tau_L^{-2}$, $n_{He\,II} \propto \tau_L^3$. Eqs. (16) and (17) can be compared with eqs. (33a) and (33b) of Deguchi (1985), which do not have the correct dependences. Also, we have used the exact spherical volume (differing by a factor of $4\pi/3$) and Doppler line width (differing by a factor of $\pi^{1/2}$). Our derived coefficients are in close agreement with those of Deguchi when his velocity dependence is removed.

VII. SUMMARY

Our discovery of O III $\lambda\lambda$3133, 3444, and possibly 3407, together with the previously known broad feature near 4640 Å, confirms the presence of Bowen fluorescence in Sco X-1. The O3 channel may be important in both the O III and the N III cascades. On the other hand, charge transfer between O IV and H I appears to be unimportant in producing any O III emission.

From the Bowen process and the absence of collisional deexcitation of He II Lyα, reasonable constraints on the density and size of the ELR are obtained. We find

$$R > 6.8 \times 10^{10} \frac{D_{700} I_{12}^{1/2}}{x_{\rm He\ III}^{1/2}} \text{ cm} , \quad (30a)$$

$$R < 3.8 \times 10^{12} \frac{D_{700}^2 I_{12}}{\tau_6^2 x_{\rm He\ III} x_{e10}} \text{ cm} \quad (30b)$$

and

$$n_e > 8.7 \times 10^6 \frac{\tau_6^3 x_{\rm He\ III} x_{e10}^2}{I_{12} D_{700}^2} \text{ cm}^{-3} , \quad (31a)$$

$$n_e < 3.7 \times 10^{10} \frac{x_{\rm He\ III}^{1/4} x_{e10}^{1/2}}{I_{12}^{1/4} D_{700}^{1/2}} \text{ cm}^{-3} , \quad (31b)$$

where D_{700} is the distance to Sco X-1 in units of 700 pc, I_{12} is our measured λ4686 intensity in units of 12×10^{-14} ergs cm^{-2} s^{-1}, τ_6 is the Lyα optical depth in units of 10^6, $x_{\rm He\ III} = n_{\rm He\ III}/n_{\rm He\ II}$, and $x_{e10} = n_e/10 n_{\rm He\ II}$. The values of R and n_e are related; an exact determination of either one completely specifies the other (§ VI). We have compared our data for Sco X-1 with an appropriate X-ray nebular model, and have found a radius for the He III Strömgren sphere (for the derived n_e) to be larger than the characteristic dimensions of the binary system. This suggests that the ELR is a low-density fringe of a more dense feature.

In addition to the Bowen lines, Sco X-1 appears to exhibit substantial Fe II emission. The Paschen decrement is quite flat, as is the Balmer decrement. Sco X-1 lies in a region of lower than average UV extinction. We find $E_{B-V} \approx 0.2$. The distance (D) to the source is given by $250 < D < 1400$ pc.

Our study, the first to probe the near-UV spectrum of Sco X-1, poses challenging questions. Further work will provide greater insight into the accretion physics of this source.

This research was supported by grants from the California Space Institute, the Institute for Geophysics and Planetary Physics at Lawrence Livermore National Laboratory, and the National Aeronautics and Space Administration Innovative Research Fund. We thank Tim Kallman for useful discussions, and Dave Neufeld, Chris McKee, Roger Romani, and Michael Strauss for making valuable comments on an earlier version of this paper. We also thank the referee, Dick McCray, for useful suggestions. Help with the observations was provided by the day and night assistants at Lick Observatory, which is partly supported by National Science Foundation Core Block grant 86-14510 to the University of California.

REFERENCES

Adams, T. F. 1972, *Ap. J.*, **174**, 439.
Aller, L. H., Bowen, I. S., and Minkowski, R. 1955, *Ap. J.*, **122**, 62.
Aller, L. H., Bowen, I. S., and Wilson, O. L. 1963, *Ap. J.*, **138**, 1013.
Bless, R. C., and Savage, D. 1972, *Ap. J.*, **171**, 193.
Boksenberg, A., *et al.* 1973, *M.N.R.A.S.*, **163**, 291.
Bopp, B. W., and Vanden Bout, P. A. 1972, *Pub. A.S.P.*, **84**, 68.
Bowen, I. S. 1934, *Pub. A.S.P.*, **46**, 146.
———. 1935, *Ap. J.*, **81**, 1.
Brocklehurst, M. 1971, *M.N.R.A.S.*, **153**, 471.
Canizares, C. R., McClintock, J. E., and Grindlay, J. E. 1979, *Ap. J.*, **234**, 556 (CMG).
———. 1980, *Ap. J. (Letters)*, **236**, L55.
Cardelli, J. A., and Savage, B. D. 1988, *Ap. J.*, **325**, 864.
Charles, P., Thorstensen, J. R., and Barr, P. 1980, *Ap. J.*, **241**, 1148.
Cowley, A. P., and Crampton, D. 1975, *Ap. J. (Letters)*, **201**, L65 (CC).
Crampton, D., Cowley, A. P., Hutchings, J. B., and Kaat, C. 1976, *Ap. J.*, **207**, 907 (CCHK).
Dalgarno, A., Heil, T. G., and Butler, S. E. 1981, *Ap. J.*, **245**, 793.
Dalgarno, A., and Sternberg, A. 1982, *M.N.R.A.S.*, **200**, 77P.
Davidson, K., and Netzer, H. 1979, *Rev. Mod. Phys.*, **51**, 715.
Deguchi, S. 1985, *Ap. J.*, **291**, 492; **303**, 901.
Djorgovski, S. 1984, in *Proc. NASA/SDSU Workshop in Photometry*, ed. W. Borucki, and A. Young (NASA CP-2350), p. 152.
Eastman, R. G., and MacAlpine, G. M. 1985, *Ap. J.*, **299**, 785.
Filippenko, A. V. 1982, *Pub. A.S.P.*, **94**, 715.
Filippenko, A. V., and Sargent, W. L. W. 1985, *Ap. J. Suppl.*, **57**, 503.
Fitzpatrick, E. L., and Massa, D. 1986, *Ap. J.*, **307**, 286.
Fowler, A., and Strutt, R. J. 1917, *Proc. Roy. Soc. London, A*, **93**, 577.
Giacconi, R., Gursky, H., Paolini, F. R., and Rossi, B. 1962, *Phys. Rev. Letters*, **9**, 439.
Gottlieb, E. W., Wright, E. L., and Liller, W. 1975, *Ap. J. (Letters)*, **195**, L33.
Gould, R. J., and Thakur, R. K. 1970, *Ann. Phys.*, **61**, 351.
Greenberg, J. M., and Chlewicki, G. 1983, *Ap. J.*, **272**, 563.
Hammerschlag-Hensberge, G., McClintock, J., and van Paradijs, J. 1982, *Ap. J. (Letters)*, **254**, L1.
Harrington, J. P. 1972, *Ap. J.*, **176**, 127.
Hiltner, W. A., and Mook, D. E. 1970, *Ann. Rev. Astr. Ap.*, **8**, 139.
Holt, S. S., Boldt, E. A., Serlemitsos, P. J., and Karluzienski., L. J. 1976, *Ap. J. (Letters)*, **205**, L79.
Hudson, H. S., Peterson, L. E., and Schwartz, D. A. 1970, *Ap. J. (Letters)*, **159**, L51.
Huggins, W. 1890, *Proc. Roy. Soc. London, A*, **48**, 216.
Kahn, S. M., Charles, P. A., Bowyer, S., and Blissett, R. J. 1981, *Ap. J.*, **250**, 733.
Kahn, S. M., Seward, F. D., and Chlebowski, T. 1984, *Ap. J.*, **283**, 286.
Kaler, J. B. 1976, *Ap. J. Suppl.*, **31**, 517.
Kaler, J. B., and Aller, L. H. 1964, *Ap. J.*, **139**, 1074.
Kaler, J. B., Aller, L. H., and Bowen, I. S. 1965, *Ap. J.*, **141**, 912.
Kallman, T. R. 1988, private communication.
Kallman, T. R., and McCray, R. 1980, *Ap. J.*, **242**, 615 (KM80).
———. 1982, *Ap. J. Suppl.*, **50**, 263.
Kestenbaum, H., Angel, J. R. P., Novick, R., and Cocke, W. J. 1971, *Ap. J. (Letters)*, **169**, L49.
Knude, J. 1987, *Astr. Ap.*, **171**, 289.
MacAlpine, G. M. 1981, *Ap. J.*, **251**, 465.
Mackay, C. D. 1986, *Ann. Rev. Astr. Ap.*, **24**, 255.
Malkan, M. A. 1986, *Ap. J.*, **310**, 679.
Margon, B., and Cohen, J. G. 1978, *Ap. J. (Letters)*, **222**, L33.
Massa, D. 1980, *A.J.*, **85**, 1651.
McClintock, J. E., Canizares, C. R., and Backman, D. E. 1978, *Ap. J. (Letters)*, **223**, L75.
McClintock, J. E., Canizares, C. R., and Tarter, B. E. 1975, *Ap. J.*, **198**, 641 (MCT).
Mewe, R. 1972, *Astr. Ap.*, **20**, 215.
Meyer, D. M., and Savage, B. D. 1981, *Ap. J.*, **248**, 545.
Miller, J. S., and Stone, R. P. S. 1987, *Lick Obs. Tech. Rept.*, No. 48.
Moore, C. E., Minnaert, M. G. J., and Houtgast, J. 1966, *NBS Monog.*, No. 61.
Nandy, K., Thompson, G. I., Jamar, C., Monfils, A., and Wilson, R. 1975, *Astr. Ap.*, **44**, 195.
Netzer, H., and Davidson, K. 1979, *M.N.R.A.S.*, **187**, 871.
Netzer, H., Elitzur, M., and Ferland, G. J. 1985, *Ap. J.*, **299**, 752.
Nussbaumer, H. 1971, *Ap. J.*, **170**, 93.
Oke, J. B., and Greenstein, J. C. 1971, *Ap. J.*, **211**, 872.
Oke, J. B., and Gunn, J. E. 1983, *Ap. J.*, **266**, 713.
Osterbrock, D. E. 1974, *Astrophysics of Gaseous Nebulae* (San Francisco: Freeman).
———. 1981, *Ap. J.*, **246**, 696.
Pengelly, R. M. 1964, *M.N.R.A.S.*, **127**, 145.
Petro, L., Bradt, H., Kelley, R., Horne, K., and Gomer, R. 1981, *Ap. J. (Letters)*, **251**, L7.
Phillips, M. M. 1978, *Ap. J. Suppl.*, **38**, 187.
Rybicki, G. B., and Lightman, A. P. 1979, *Radiative Processes in Astrophysics* (New York: Wiley).
Sandage, A. R., *et al.* 1966, *Ap. J.*, **146**, 316.
Saraph, H. E., and Seaton, M. J. 1980, *M.N.R.A.S.*, **193**, 617 (SS).

Savage, B. D., and Mathis, J. S. 1979, *Ann. Rev. Astr. Ap.*, **17**, 73.
Seaton, M. J. 1978, *M.N.R.A.S.*, **185**, 5P.
Shuder, J. M., and MacAlpine, G. M. 1979, *Ap. J.*, **230**, 348.
Shuder, J. M., and Osterbrock, D. E. 1981, *Ap. J.*, **250**, 55.
Sternberg, A., and Dalgarno, A. 1989, *Ap. J.*, **338**, 197.
Stirpe, G. M., de Bruyn, A. G., and van Groningen, E. 1988, *Astr. Ap.*, **200**, 9.
Stone, R. P. S. 1977, *Ap. J.*, **218**, 767.
Striganov, A. R., and Sventitskii, N. S. 1968, *Tables of Spectral Lines of Neutral and Ionized Atoms* (New York: Plenum).
Wade, R. A., and Horne, K. D. 1988, *Ap. J.*, **324**, 411.
Wallerstein, G. 1967, *Ap. Letters*, **1**, 31.
Weymann, R. J., and Williams, R. E. 1969, *Ap. J.*, **157**, 1201.
Whelan, J. A. J., *et al.* 1977, *M.N.R.A.S.*, **180**, 657.
Willis, A. J., *et al.* 1980, *Ap. J.*, **237**, 596.

ALEXEI V. FILIPPENKO: Department of Astronomy, University of California, Berkeley, CA 94720
[BITNET: alex%bkyast@ucbjade, INTERNET: alex@bkyast.berkeley.edu, SPAN: 42215::alex]

STEVEN M. KAHN and JONATHAN SCHACHTER: Department of Physics, University of California, Berkeley, CA 94720
[BITNET: schachter%bkyast@ucbjade, INTERNET: schachter@bkyast.berkeley.edu, SPAN: 42215::schachter]